# Nonvolatile Reconfigurable Phase-Shifted Bragg Grating Filter With Tunable Wavelength and Extinction Ratio

Wenfei Li, Chao Qiu, and Aimin Wu

***Abstract*—Nonvolatile compact on-chip optical filters with a tunable spectral response are required in low-power optical communication systems and applications. By capping phase change materials (PCMs) films on a phase-shifted Bragg grating (PSBG), the key parameters of a filter such as center wavelength and extinction ratio can be tuned simultaneously for filtering or processing purposes. A 9 nm wavelength shift, and amplitude modulations of 16.1 dB in the transmission channel and 42.5 dB in the reflection channel while keeping the center wavelength unchanged are achieved in this filter at 1550 nm. Moreover, the device has a compact size of 500 nm $\times$ 31.9 $\mu$m and an insertion loss as low as -0.76 dB, making it ideal for large-scale integration. The advent of such compact, reconfigurable, nonvolatile optical filters opens up new avenues for next-generation low-power general-purpose photonic integrated circuits (PICs) and has potential applications in wavelength division multiplexing (WDM) systems, spectral shaping, and on-chip signal processors.**

***Index Terms*—Silicon photonics, tunable filter, phase change materials, Bragg grating.**

## I. Introduction

As THE size of transistors continues to shrink, traditional integrated circuits are reaching the limits of their power and speed capabilities. Photonic integrated circuits (PICs) have the potential to become the next generation of computing hardware platforms due to their high speed, parallelism, and low energy consumption [1], [2], [3], [4], [5]. Silicon-based optoelectronics, which utilizes the well-developed CMOS manufacturing process, allows for the concentration of optical, electrical, and optoelectronic devices on a single silicon substrate, making it a promising approach for realizing large-scale PICs [6], [7]. Next-generation silicon-based photonic processors for photonic computing and communication networks require compact on-chip optical filters with a reconfigurable spectral response [8]. Silicon optical filters are key devices in silicon-based PICs that enable the selection of input optical wavelengths and are critical in application scenarios such as wavelength division multiplexing systems and on-chip optical signal processing.

The main technical solutions for implementing silicon optical filters in existing studies are Mach-Zehnder interferometers [9], [10], [11], micro-ring resonators [12], [13], [14], photonic crystal nanobeam microcavities [15], [16], [17], echelle diffraction gratings [18], [19] and waveguide Bragg gratings [8], [20], [21]. As a filter device with a small size and high integration, the Bragg grating has an important use in PICs and has been widely studied. The Bragg grating achieves different spectral responses by changing the period, refractive index change, phase, and other parameters of the grating in the propagation direction [22], [23]. However, the transmission characteristics of conventional Bragg grating are completely determined by the structural parameters of the device for a particular use and cannot be changed with the requirements of the application after preparation [22], [24]. These devices are often sensitive to the fabrication process and exhibit limited tolerance for small variations in manufacturing parameters. For instance, a deviation of 10 nm in the grating period, as demonstrated in ref. [22], can cause a significant wavelength shift of over 5 nm in the resonance peak. Likewise, the depth of sidewall corrugation can also impact the extinction ratio of the filter. The structural variations resulting from fabrication can lead to deviations in the transmission characteristics from the desired specifications, necessitating compensatory measures such as external thermal or electrical control, which unfortunately result in an increased power consumption. Existing reconfigurable silicon optical filters usually use thermo-optical [11] or carrier-induced electro-optical [25] effects to modulate the effective refractive index of the material, which has low modulation efficiency and introduces additional losses, and the adjustable functions are mostly limited to the wavelength shift. Therefore, the research and design of new low-power reconfigurable silicon optical filters have become one of the key technologies for the development of silicon optical integrated circuits.

Nonvolatile phase change material (PCM) is a kind of material with high optical contrast, which can be continuously adjusted between amorphous and crystalline phases by applying electrical/optical pulses of nanosecond level in a fast and repetitive

Manuscript received 20 February 2023; revised 8 April 2023; accepted 12 April 2023. Date of publication 14 April 2023; date of current version 24 April 2023. This work was supported by the National Key R&D Program of China under Grant 2021YFB2206502 and in part by Youth Innovation Promotion Association CAS under Grant 2021232. *(Corresponding author: Aimin Wu.)*

Wenfei Li is with the State Key Laboratory of Functional Materials for Informatics, Shanghai Institute of Microsystem and Information Technology, Chinese Academy of Sciences, Shanghai 200050, China, and also with the School of Physical Science and Technology, Shanghaitech University, Shanghai 201210, China (e-mail: liwf@shanghaitech.edu.cn).

Chao Qiu and Aimin Wu are with the State Key Laboratory of Functional Materials for Informatics, Shanghai Institute of Microsystem and Information Technology, Chinese Academy of Sciences, Shanghai 200050, China, and also with the Center of Materials Science and Optoelectronics Engineering, University of Chinese Academy of Sciences, Beijing 100049, China (e-mail: cqiu@mail.sim.ac.cn; wuaimin@mail.sim.ac.cn).

Digital Object Identifier 10.1109/JPHOT.2023.3267276

manner [26], [27], [28], [29], and the final material properties can be maintained even after the external excitation is turned off. Introducing nonvolatile PCMs with specific optical properties in conventional silicon optical filters can realize multi-functional reconfigurable silicon optical filters with zero static power consumption. Ge $_2$ $Sb_2Te_5$ (GST) has been employed in Bragg grating filters to achieve reconfigurable performance [30], [31], but the large extinction coefficient of GST results in significant insertion loss in the filter. Periodic GST structures placed on the outer side of waveguides have introduced an insertion loss of -1.14 dB to the device [31]. Even with a very small area, direct integration of GST onto waveguides has led to insertion loss as high as -2.64 dB [30]. $Sb_2Se_3$ and $Ge_2$ $Sb_2Se_4$ $Te_1$ (GSST) are newly developed PCMs with optical transparency at communication wavelengths. Their extinction coefficients in the amorphous state are lower by 3-5 orders of magnitude compared to GST, making them more suitable for low-loss optical devices [32], [33].

In this work, an on-chip nonvolatile reconfigurable Bragg grating filter capped with Sb $_2$ $Se_3$ and GSST is proposed and numerically simulated. The proposed filter shows an insertion loss of -0.76 dB, a 9 nm wavelength shift with amplitude modulation of 16.1 dB in the transmission channel and 42.5 dB in the reflection channel at 1550 nm.

## II. Principle and Design

Traditional uniform Bragg gratings achieve a periodic arrangement of effective refractive index variations by periodically varying the dielectric waveguide structure, which reflects certain wavelengths of input light while allowing others to pass through. Introducing a quarter-wave phase shift in the central region of a Bragg grating will result in a resonant mode at the Bragg wavelength that manifests as a narrow peak on the transmission spectrum which is called phase-shifted Bragg grating (PSBG) [34]. Here we choose to introduce two kinds of nonvolatile PCMs, GSST placed at the phase-shifted region and Sb $_2$ $Se_3$ at both sides of the PSBG. The multifunctional nonvolatile reconfigurable filter is realized by modulating the crystalline state of the PCM in each region corresponding to the effective refractive index of the waveguide. The switching of phase change materials can achieve fine phase control at the hundreds nanometer pixel level by using tightly focused optical pulses [35]. The refractive index (blue) and extinction coefficient (orange) of the two PCMs extracted from ref. [36], [37] are shown in Fig. 1. In the telecommunication band, the refractive indexes for both of them are comparable with that of silicon in the amorphous state and have a significant contrast between the amorphous and crystalline states. The extinction coefficient of Sb $_2$ $Se_3$ has particularly low absorptions ($\sim$1e $^{-6}$) in both amorphous state and crystalline state while GSST is more absorptive in the crystalline state at 1550 nm. The lossless property of $Sb_2$ $Se_3$ is used to change the transmission effective refractive index of the waveguide to control the shift of the resonant peak wavelength, and the gradual increase of the loss from amorphous to the crystalline state of GSST is used to attenuate the resonant peak intensity, and the superposition

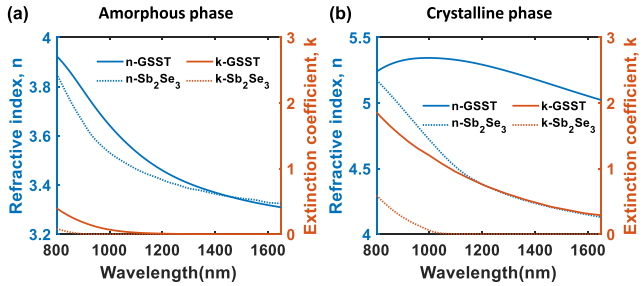


Fig. 1. Material optical properties (n and k) of GSST (solid lines) and Sb $_2$ $Se_3$ (dashed lines) in (a) amorphous state and (b) crystalline state at the wavelength from 800 nm to 1650 nm. The blue curves represent the refractive index n, and the orange curves are the extinction coefficient k.

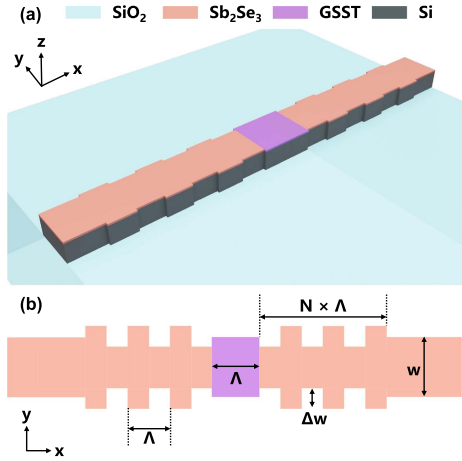


Fig. 2. Designed nonvolatile reconfigurable Bragg filter. (a) schematic diagram of the filter based on phase-shifted waveguide Bragg grating. (b) top view of the filter. N: number of the grating; $\Delta$w: sidewall corrugation depth; $\Lambda$: grating period; w: average waveguide width.

of the two effects achieves the simultaneous adjustment of the resonant peak wavelength and extinction ratio. In the crystalline and amorphous states, only the real part of the refractive index of $Sb_2$ $Se_3$ changes, and the imaginary part of the refractive index is always zero, which means that it does not absorb the incident light, and the resonance peak can be shifted by tuning its state without bringing additional losses. The absorption coefficient of GSST becomes larger with increasing crystallinity and can be used to tune the incident light attenuation and thus realize the control of the incident light intensity.

Fig. 2 depicts the three-dimensional structure diagram of the proposed Bragg grating filter structure. A normal PSBG waveguide is covered by Sb $_2$ $Se_3$ films in the uniform grating regions and a GSST film in the phase-shifted region, which is designed to maintain the symmetry of the Bragg grating waveguide filter. In the design, the silicon waveguide has a width of w = 500 nm and thickness of h = 220 nm allowing single-mode operation [38]. As for Bragg grating, the center Bragg wavelength is determined by both the waveguide refractive index and the grating period which fulfills the Bragg condition [39],

$$\lambda_B = 2n_{eff}\Lambda, \tag{1}$$

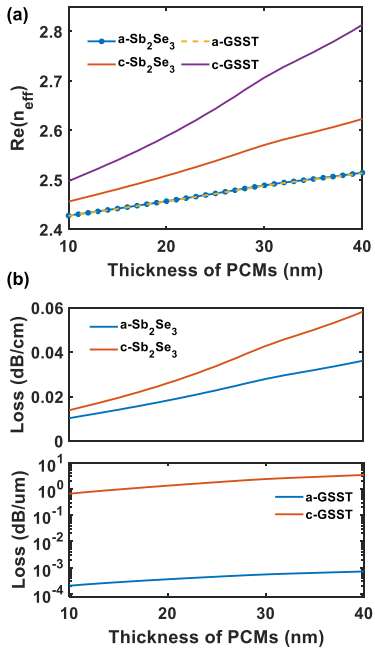


Fig. 3. Si-PCM hybrid waveguide (a) effective refractive index (Re($n_{eff}$)) and (b) propagation loss of fundamental quasi-TE mode with varying thickness of PCMs at 1550 nm.

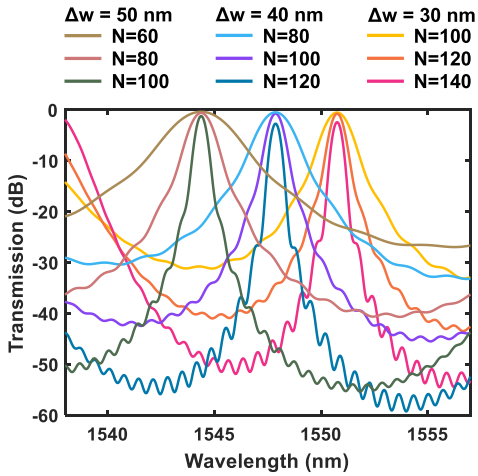


Fig. 4. Effect of sidewall corrugation depth (Δw) and number of the grating (N) on the transmission spectra of PSBG filter.

where $\lambda_B$ is the Bragg wavelength, $n_{eff}$ is the effective refractive index of the waveguide and $\Lambda$ is the grating period.

In Fig. 3(a), the effective refractive indices of Si-PCM hybrid waveguides with different PCM thicknesses for fundamental transverse electric ($TE_0$) mode are calculated using the finite-difference eigen-mode (FDE) method in Lumerical Mode. The $n_{eff}$ of both PCMs in the crystalline and amorphous states increases with their thicknesses. In the amorphous state, the hybrid waveguides formed by the same thickness of $Sb_2Se_3$ and GSST have almost the same $n_{eff}$. The extinction coefficient of $Sb_2Se_3$ is near zero in any state and is suitable for filter wavelength adjustment with low losses. The large optical contrast and absorption capability of GSST in the crystalline state make it proper for the output optical power adjustment of a filter. The propagation losses of these Si-PCM hybrid waveguides as a function of PCM thickness are also plotted in Fig. 3(b) which can be predicated by:

$$loss = -20log_{10}\left(e^{-2\pi\kappa/\lambda_0}\right), \tag{2}$$

where $\kappa$ is the imaginary part of $n_{eff}$. In the designed filter, both $Sb_2Se_3$ and GSST films were chosen to be 20 nm thick for offering large modulation range with moderate insertion loss. For the hybrid waveguide capped with a 20-nm-thick PCM film, there is an effective refractive index modification of 0.05 for $Sb_2Se_3$ and 0.13 for GSST, respectively from the amorphous to the crystalline state. As shown in Fig. 3(a), the $n_{eff}$ of the 20-nm-thick $Sb_2Se_3$ film in the amorphous state of the hybrid waveguide is 2.45. Therefore, to facilitate operation at 1550 nm, the grating period of this filter should be chosen as $\Lambda = 316$ nm according to the Bragg condition. The transmissivity and bandwidth (Q-factor) of the Bragg grating filter are related as follows [40]:

$$T_{\max} = \left(\frac{Q}{Q_T}\right)^2, \tag{3}$$

where $1/Q = 1/Q_T + 1/Q_L$, $Q_T$ is the quality factor of the resonator, $Q_L$ is the dissipation quality factor induced by loss and $T_{max}$ is the maximum transmission. Hence, a trade-off between the Q-factor and transmissivity exists in the design of Bragg gratings to achieve high transmissivity with narrow bandwidth, i.e. there should be a compromise between the number of grating periods (N) and grating coupling factor, which is a function of grating etch depth (Δ w). By reducing the grating length and increasing the sidewall corrugation depth to increase the coupling factor, a more compact design can be obtained.

The effects of sidewall corrugation depth and the number of grating periods on the designed filter are theoretically investigated by 3D finite-difference-time-domain (FDTD) simulation. Fig. 4 shows that as the number of periods increases, the bandwidth becomes narrower, but the transmissivity drops at the same time, and the increase of the waveguide sidewall corrugation depth can improve the coupling coefficient of the grating, but meanwhile, it also brings transmission losses. In other words, the grating with a longer length and deeper waveguide sidewall corrugation depth can provide a narrower bandwidth at the expense of transmissivity. The filter employs 50 of Bragg gratings periods ($N = 50$) on each side of the phase-shifted region (resulting in a length of 31.9 Âμm) and a sidewall corrugation depth of $\Delta w = 40$ nm to achieve a balance between low loss transmission and narrow bandwidth filter characteristics.

To prepare the PCM thin film on the waveguide in the filter, a two-step process involving electron beam lithography and lift-off can be employed. Firstly, a window is opened on the waveguide through electron beam lithography. Subsequently, PCM films are deposited using a radio-frequency sputtering system. Finally, the lift-off process is performed to remove the unwanted PCM, leaving behind the desired PCM thin films on

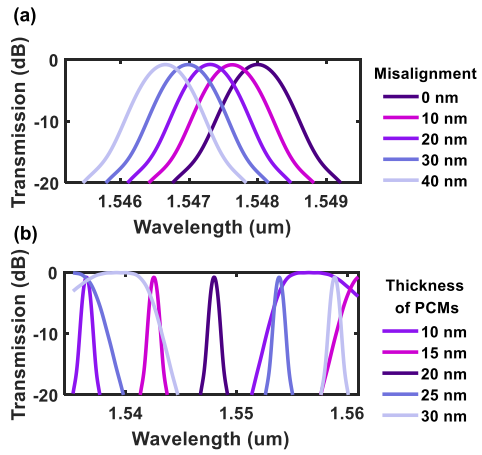


Fig. 5. Effect of (a) misalignment and (b) thickness of PCMs on the transmission spectra of PSBG filter. The deepest purple line represents the transmission spectra of designed filter.

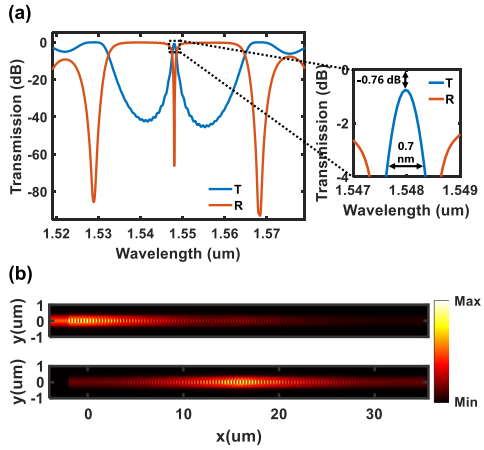


Fig. 6. (a) Spectral responses of the designed filter. T: transmission, R: reflection. Right inset: Magnified view of the transmission resonance peak. (b) Electric field profiles at the wavelength of minimum (top) and maximum (bottom) transmission.

the waveguide. It is worth noting that our previous work has demonstrated the feasibility of capping PCM films on silicon waveguide with a misalignment below 20 nm [41]. The effects of the misalignment or thickness variation on the designed filter are also calculated and depicts in Fig. 5. These variations can affect the effective refractive index of the waveguide, resulting in a shift of the transmission resonant peak in the filter, but do not affect the transmission spectrum bandwidth and loss. The resonance wavelength shift caused by alignment errors within a certain range can be compensated for by the tunability of the device. Additionally, tunable filters with different operating wavelengths can be achieved through the use of PCMs with varying thicknesses. The thickness of the PCM can be controlled by pre-testing the thin film sputtering rate of the radio-frequency sputtering system.

## III. Results and Discussion

The transmission and reflection spectra of the designed filter are presented in Fig. 6(a), where a resonant window appears in the center of the transmission stopband. The right inset plot provide a magnified view of the transmission spectrum, indicating a 3-dB bandwidth of 0.7 nm and an insertion loss of -0.76 dB. The insertion loss is calculated by normalizing the resonant peak power to the source power. Fig. 6(b) shows the simulated propagation of the maximum and minimum transmission of input light in the designed Bragg filter at different wavelengths. The quarter-wave spacing in the center of the waveguide forms a resonant microcavity, and the strong field that appears here indicates that the light is undergoing strong resonance.

In addition to high contrast refractive index modulation, a multilevel or multi-bit operation can be obtained using PCMs [26], [42]. The PCM can be converted to a partially crystalline state by heating the GST to a temperature just above its crystallization temperature but below its melting point by a sufficiently long sequence of short pulses or a single long pulse [43]. The partial crystalline state contains different proportions of mutually interspersed crystalline and amorphous phases, both of which are capable of stable existence [29]. The Lorentz-Lorenz relation can be used to approximate the effective permittivity $\varepsilon_{eff}$ ($\lambda$) of the PCM film in the partially crystalline state as follows [44],

$$\frac{\varepsilon_{eff}(\lambda)-1}{\varepsilon_{eff}(\lambda)+2} = f \times \frac{\varepsilon_{cPCM}(\lambda)-1}{\varepsilon_{cPCM}(\lambda)+2} + (1-f) \times \frac{\varepsilon_{aPCM}(\lambda)-1}{\varepsilon_{aPCM}(\lambda)+2}, \quad (4)$$

where f is the crystalline fraction of PCM, $\varepsilon_{cPCM}$ is the permittivity of PCM in the crystalline state and $\varepsilon_{aPCM}$ is the permittivity of PCM in the amorphous state. Precise control of the partially crystalline state phase composition can be achieved by varying the crystallizing pulse duration or voltage, thus enabling quasi-continuous tuning of the filter performance.

### A. Quasi-Continuous Bragg Wavelength Tuning of the Filter

According to (1), the Bragg wavelength of the Bragg grating filter depends mainly on the period of the grating and the effective refractive index of the waveguide. When the filter is manufactured, the structural parameters are already determined and cannot be changed, so the Bragg wavelength of the grating filter can only be modulated by adjusting the refractive index of the waveguide. It is usually desired to keep the transmitted optical power of the filter as constant as possible while using the wavelength tuning function, thus the Bragg wavelength tuning is achieved only by changing the degree of crystallization of the near-zero absorptivity $Sb_2Se_3$ film and maintaining the GSST film on the waveguide always in the amorphous state with the lowest absorbance. Fig. 7 shows the quasi-continuous Bragg wavelength tuning in the transmission spectrum (top) and the reflection spectrum (bottom) when the degree of crystallization of the $Sb_2Se_3$ film covering the waveguide of the left and right subsegment grating is varied simultaneously. The change in the

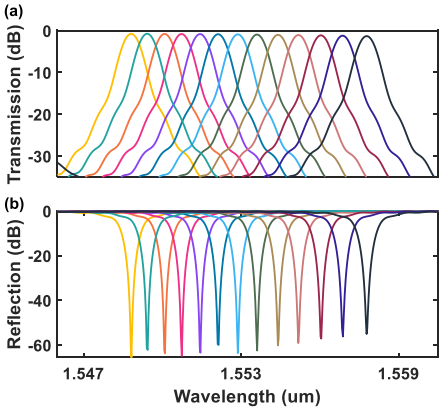


| line | crystallization fraction (%) | | |
|---|---|---|---|
| | $Sb_2Se_3$ - left | $Ge_2Sb_4Se_4Te_1$ | $Sb_2Se_3$ - right |
| | 0 | 0 | 0 |
| | 5 | 0 | 5 |
| | 10 | 0 | 10 |
| | 15 | 0 | 15 |
| | 20 | 0 | 20 |
| | 25 | 0 | 25 |
| | 30 | 0 | 30 |
| | 35 | 0 | 35 |
| | 40 | 0 | 40 |
| | 45 | 0 | 45 |
| | 50 | 0 | 50 |
| | 55 | 0 | 55 |
| | 60 | 0 | 60 |

Fig. 7. The quasi-continuous Bragg wavelength tuning with different crystallization fractions applied to the left and right subsegment gratings synchronously. (a) Transmission spectra; (b) Reflection spectra.

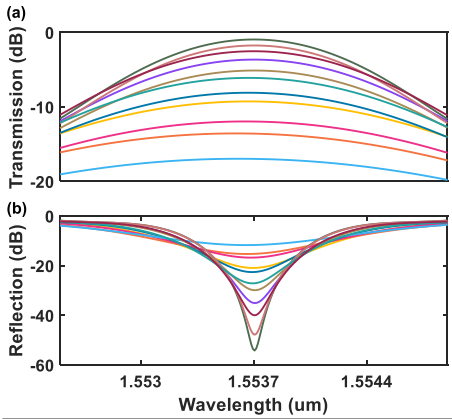


| line | crystallization fraction (%) | | |
|---|---|---|---|
| | $Sb_2Se_3$ - left | $Ge_2Sb_4Se_4Te_1$ | $Sb_2Se_3$ - right |
| | 18 | 0 | 52 |
| | 25 | 10 | 45 |
| | 7 | 20 | 58 |
| | 12 | 30 | 53 |
| | 20 | 40 | 45 |
| | 5 | 50 | 55 |
| | 13 | 60 | 47 |
| | 0 | 70 | 55 |
| | 10 | 80 | 45 |
| | 0 | 90 | 50 |
| | 15 | 100 | 35 |

Fig. 8. The quasi-continuous extinction ratio tuning while keeping the center wavelength unchanged with different crystallization fractions combinations applied to the left, center, and right subsegment of the filter. (a)Transmission spectra; (b) Reflection spectra.

crystallization fraction of the $Sb_2Se_3$ film causes a change in the effective refractive index of the transmitting waveguide, which results in a shift in the Bragg wavelength. As the degree of crystallization of the $Sb_2Se_3$ film increases, the transmission peak in the spectral response is red-shifted. The Bragg wavelength of the Bragg grating filter achieves a shift of up to 9 nm from 1549 nm to 1558 nm as the degree of crystallization of the $Sb_2Se_3$ film covered on the waveguide of the left and right subsegment gratings gradually changes from 0% to 60% in steps of 5%. A larger wavelength tuning range can be obtained by introducing an assisted thermal tuning structure.

### *B. Quasi-Continuous Extinction Ratio Tuning of the Filter*

In the existing studies of tunable extinction ratio filters, the resonance peak of the resonant cavity is generally shifted to achieve the adjustment of the extinction ratio at the original resonance wavelength [30], but this method does not really achieve the attenuation of the resonance peak and introduces additional crosstalk to the adjacent wavelength channels in the wavelength division multiplexing (WDM) system. The GSST film covering waveguides in the phase-shifting region can change from the near-zero absorption characteristics of the amorphous state to the lossy characteristics of the crystalline state, which is used in this work to achieve the tuning of the filter extinction ratio. However, only changing the crystallinity of GSST film can attenuate the output optical power of the filter, but it also changes the Bragg wavelength of the filter. In the proposed multiple-region-tunable filter, the wavelength shift caused by the change in the crystallinity of the GSST film in the phase-shifted region can be offset by simultaneously tuning the crystallinity of $Sb_2Se_3$ film in each of the two subsegment regions. Thus, applying different combinations of crystallization fractions to the designed filter can result in different round-trip losses, thus achieving different extinction ratios while keeping the central wavelength constant. Fig. 8 shows the transmission (top) and reflection (bottom) spectra of the quasi-continuous extinction ratio tuning. During the tuning process, the crystallinity of the GSST film gradually increases from 0% to 100% in steps of 10%, and the total crystallinity of the $Sb_2Se_3$ film then gradually decreases to compensate for the Bragg wavelength redshift caused by the increase in refractive index of the GSST film. The crystallinity of the $Sb_2Se_3$ films on the left and right sides is distributed with the goal of aligning the central wavelength, and the larger the difference in crystallinity between the two sides brings a larger Bragg wavelength redshift. In the transmission channel, the maximum optical power is -0.9 dB when the crystallization fraction combination is 18% in the left subsegment grating, 0% in the central subsegment, and 52% in the right subsegment

TABLE I
COMPARISON AMONG TUNABLE OPTICAL FILTERS

| References | Tuning scheme | Footprint | Nonvolatility | Insertion Loss | Wavelength Tuning Range | Extinction Ratio Tuning Range |
|---|---|---|---|---|---|---|
| [8] | Electrical | 0.3 $mm^2$ | volatile | -20.6 dB (including coupling loss) | 431 pm | 8.9 dB |
| [20] | Thermal | 137.5 $\mu m^2$ | volatile | -5 dB | 2 nm | - |
| [30] | PCM | 10.2 $\mu m^2$ | nonvolatile | -2.64 dB | 8.8 nm | 24 dB (center wavelength changed) |
| [31] | PCM | 24.3 $\mu m^2$ | nonvolatile | -1.14 dB | 4 nm | 28.8 dB (center wavelength changed) |
| This work | PCM | 16 $\mu m^2$ | nonvolatile | -0.76 dB | 9 nm | 16.1 dB in transmission channel / 42.5 dB in reflection channel |

grating, while the minimum optical power is -17.0 dB and the extinction ratio is 16.1 dB when the crystallization fraction combination is 15% in the left subsegment grating, 100% in the central subsegment, and 35% in the right subsegment grating. In the reflection channel, the maximum optical power is -11.7 dB, the minimum optical power is -54.2 dB, and the extinction ratio is 42.5 dB. A comparison between our proposed tunable filter and prior literature is summarized in Table I, highlighting our advantages in terms of device footprint, nonvolatility, insertion loss, and tuning capability. Tuning extinction ratio with constant central wavelength is a unique and advantageous feature of the designed filter, which can be applied to channel gain equalization in WDM systems.

## IV. CONCLUSION

In conclusion, a nonvolatile reconfigurable PSBG filter with tunable wavelength and extinction ratio is illustrated in this work. This filter capped with PCMs can operate wavelength tuning with low transmission loss and extinction ratio tuning at a specific wavelength in a single device by properly selecting the crystalline fraction combination of PCMs. A 9 nm redshift with amplitude modulation of 16.1 dB (transmission channel) / 42.5 dB (reflection channel) is achieved in the filter at 1550 nm. The insertion loss of this filter is -0.76 dB. Benefiting from the nonvolatile properties of the PCMs, any of the filter's propagation states can be maintained without depleting additional energy after the external supply is turned off. Moreover, the operation wavelength band can be reconfigured by designing the device structure parameters. The availability of such a compact, reconfigurable, and nonvolatile optical filter can find many applications in WDM systems, spectral shaping, and on-chip signal processors.

## REFERENCES


[1] B. J. Shastri et al., "Photonics for artificial intelligence and neuromorphic computing," *Nature Photon.*, vol. 15, no. 2, pp. 102–114, 2021.

[2] P. Stark, F. Horst, R. Dangel, J. Weiss, and B. J. Offrein, "Opportunities for integrated photonic neural networks," *Nanophotonics*, vol. 9, no. 13, pp. 4221–4232, 2020.

[3] W. Bogaerts et al., "Programmable photonic circuits," *Nature*, vol. 586, no. 7828, pp. 207–216, 2020.

[4] Q. Zhang, H. Yu, M. Barbiero, B. Wang, and M. Gu, "Artificial neural networks enabled by nanophotonics," *Light: Sci. Appl.*, vol. 8, no. 1, 2019, Art. no. 42.

[5] D. Pérez, I. Gasulla, P. Das Mahapatra, and J. Capmany, "Principles, fundamentals, and applications of programmable integrated photonics," *Adv. Opt. Photon.*, vol. 12, no. 3, pp. 709–786, 2020.

[6] T. Tsuchizawa et al., "Monolithic integration of silicon photonics devices for telecommunications applications," *NTT Tech. Rev.*, vol. 9, no. 5, pp. 1–10, 2011.

[7] K. Yamada et al., "High-performance silicon photonics technology for telecommunications applications," *Sci. Technol. Adv. Mater.*, vol. 15, no. 2, Apr. 2014, Art. no. 0 24603.

[8] W. Zhang and J. Yao, "A fully reconfigurable waveguide Bragg grating for programmable photonic signal processing," *Nature Commun.*, vol. 9, no. 1, pp. 1–9, 2018.

[9] Q. Sun, L. Zhou, L. Lu, G. Zhou, and J. Chen, "Reconfigurable high-resolution microwave photonic filter based on dual-ring-assisted MZIs on the $Si_3N_4$ platform," *IEEE Photon. J.*, vol. 10, no. 6, pp. 1–12, Dec. 2018.

[10] H. Xu, D. Dai, and Y. Shi, "Low-crosstalk and fabrication-tolerant four-channel CWDM filter based on dispersion-engineered Mach-Zehnder interferometers," *Opt. Exp.*, vol. 29, no. 13, pp. 20617–20631, 2021.

[11] A. P. Ovvyan, N. Gruhler, S. Ferrari, and W. H. P. Pernice, "Cascaded Mach–Zehnder interferometer tunable filters," *J. Opt.*, vol. 18, no. 6, Jun. 2016, Art. no. 64011.

[12] M. S. Dahlem, C. W. Holzwarth, A. Khilo, F. X. Kärtner, H. I. Smith, and E. P. Ippen, "Reconfigurable multi-channel second-order silicon microring-resonator filterbanks for on-chip WDM systems," *Opt. Exp.*, vol. 19, no. 1, pp. 306–316, 2011.

[13] S. Park, K.-J. Kim, I.-G. Kim, and G. Kim, "Si micro-ring MUX/DeMUX WDM filters," *Opt. Exp.*, vol. 19, no. 14, pp. 13531–13539, 2011.

[14] P. De Heyn et al., "Fabrication-tolerant four-channel wavelength-division-multiplexing filter based on collectively tuned Si microrings," *J. Lightw. Technol.*, vol. 31, no. 16, pp. 2785–2792, Aug. 2013.

[15] Y. Zhang et al., "Single-resonance silicon nanobeam filter with an ultra-high thermo-optic tuning efficiency over a wide continuous tuning range," *Opt. Lett.*, vol. 43, no. 18, pp. 4518–4521, 2018.

[16] Z. Cheng, J. Zhang, J. Dong, and Y. Ding, "Compact high-contrast silicon optical filter using all-passive and CROW Fano nanobeam resonators," *Opt. Lett.*, vol. 46, no. 16, pp. 3873–3876, 2021.

[17] D. Yang, C. Wang, and Y. Ji, "Silicon on-chip one-dimensional photonic crystal nanobeam bandgap filter integrated with nanobeam cavity for accurate refractive index sensing," *IEEE Photon. J.*, vol. 8, no. 2, pp. 1–8, Apr. 2016.

[18] F. Horst, "Silicon integrated waveguide devices for filtering and wavelength demultiplexing," in *Proc. IEEE Opt. InfoBase Conf. Papers*, 2010, pp. 1–3.

[19] J. Brouckaert, W. Bogaerts, P. Dumon, D. Van Thourhout, and R. Baets, "Planar concave grating demultiplexer fabricated on a nanophotonic silicon-on-insulator platform," *J. Lightw. Technol.*, vol. 25, no. 5, pp. 1269–1275, May 2007.

[20] M. Khalil, H. Sun, E. Berikaa, D. V. Plant, and L. R. Chen, "Electrically reconfigurable waveguide Bragg grating filters," *Opt. Exp.*, vol. 30, no. 22, pp. 39643–39651, 2022.

[21] H. Qiu et al., "Silicon add-drop filter based on multimode Bragg sidewall gratings and adiabatic couplers," *J. Lightw. Technol.*, vol. 35, no. 9, pp. 1705–1709, May 2017.

[22] P. Prabhathan, V. M. Murukeshan, Z. Jing, and P. V. Ramana, "Compact SOI nanowire refractive index sensor using phase shifted Bragg grating," *Opt. Exp.*, vol. 17, no. 17, pp. 15330–15341, 2009.

[23] C. Husko, A. Ducharme, N. M. Fahrenkopf, and J. R. Guest, "Phase-shifted Bragg gratings in a foundry silicon nitride platform," *OSA Continuum*, vol. 4, no. 3, pp. 933–939, 2021.

[24] X. Wang, S. Grist, J. Flueckiger, N. A. F. Jaeger, and L. Chrostowski, "Silicon photonic slot waveguide Bragg gratings and resonators," *Opt. Exp.*, vol. 21, no. 16, pp. 19029–19039, 2013.

[25] J. Yao and W. Zhang, "Fully reconfigurable waveguide Bragg gratings for programmable photonic signal processing," *J. Lightw. Technol.*, vol. 38, no. 2, pp. 202–214, Jan. 2020.

[26] X. Li et al., "Fast and reliable storage using a 5 bit, nonvolatile photonic memory cell," *Optica*, vol. 6, no. 1, pp. 1–6, 2019.

[27] C. Rios et al., "Controlled switching of phase-change materials by evanescent-field coupling in integrated photonics [Invited]," *Opt. Mater. Exp.*, vol. 8, no. 9, pp. 2455–2470, 2018.
[28] B. Gholipour, "The promise of phase-change materials," *Science*, vol. 366, no. 6462, pp. 186–187, Oct. 2019.
[29] C. Rios et al., "Integrated all-photonic non-volatile multi-level memory," *Nature Photon.*, vol. 9, no. 11, pp. 725–732, Nov. 2015.
[30] S. H. Badri, M. M. Gilarlue, S. G. Farkoush, and S.-B. Rhee, " Reconfigurable bandpass optical filters based on subwavelength grating waveguides with a $Ge_2Sb_2Te_5$ cavity," *J. Opt. Soc. Amer. B*, vol. 38, no. 4, pp. 1283–1289, Apr. 2021.
[31] S. H. Badri and S. G. Farkoush, "Subwavelength grating waveguide filter based on cladding modulation with a phase-change material grating," *Appl. Opt.*, vol. 60, no. 10, pp. 2803–2810, 2021.
[32] Y. Zhang et al., "Broadband transparent optical phase change materials for high-performance nonvolatile photonics," *Nature Commun.*, vol. 10, no. 1, pp. 1–9, 2019.
[33] M. Delaney, I. Zeimpekis, D. Lawson, D. W. Hewak, and O. L. Muskens, "A new family of ultralow loss reversible phase-change materials for photonic integrated circuits: $Sb_2S_3$ and $Sb_2Se_3$," *Adv. Funct. Mater.*, vol. 30, no. 36, 2020, Art. no. 2002447.
[34] M. H. Asghari and J. Azaña, "Design of all-optical high-order temporal integrators based on multiple-phase-shifted Bragg gratings," *Opt. Exp.*, vol. 16, no. 15, pp. 11459–11469, Jul. 2008.
[35] M. Delaney et al., "Nonvolatile programmable silicon photonics using an ultralow-loss $Sb_2Se_3$ phase change material," *Sci. Adv.*, vol. 7, no. 25, pp. 1–8, 2021.
[36] T. Zhou et al., "Reconfigurable hybrid silicon waveguide Bragg filter using ultralow-loss phase-change material," *Appl. Opt.*, vol. 61, no. 7, pp. 1660–1667, 2022.
[37] Q. Zhang, Y. Zhang, J. Li, R. Soref, T. Gu, and J. Hu, "Broadband nonvolatile photonic switching based on optical phase change materials: Beyond the classical figure-of-merit," *Opt. Lett.*, vol. 43, no. 1, p. 94–97, 2018.
[38] L. Chrostowski and M. Hochberg, *Silicon Photonics Design: From Devices to Systems*. Cambridge, U.K.: Cambridge Univ. Press, 2015.
[39] F. Kehl, D. Bischof, M. Michler, M. Keka, and R. Stanley, "Design of a label-free, distributed Bragg grating resonator based dielectricwaveguide biosensor," *Photonics*, vol. 2, no. 1, pp. 124–138, Jan. 2015.
[40] M. Rattier et al., "Performance of waveguide-based two-dimensional photonic-crystal mirrors studied with Fabry-Perot resonators," *IEEE J. Quantum Electron.*, vol. 37, no. 2, pp. 237–243, Feb. 2001.
[41] W. Li et al., "Ultracompact high-extinction-ratio nonvolatile on-chip switches based on structured phase change materials," *Laser Photon. Rev.*, vol. 16, no. 6, pp. 1–6, 2022.
[42] J. Zheng et al., "GST-on-silicon hybrid nanophotonic integrated circuits: A non-volatile quasi-continuously reprogrammable platform," *Opt. Mater. Exp.*, vol. 8, no. 6, pp. 1551–1561, 2018.
[43] J. Von Keitz et al., "Reconfigurable nanophotonic cavities with nonvolatile response," *ACS Photon.*, vol. 5, no. 11, pp. 4644–4649, Nov. 2018.
[44] Y. G. Chen et al., "Hybrid phase-change plasmonic crystals for active tuning of lattice resonances," *Opt. Exp.*, vol. 21, no. 11, pp. 13691–13698, 2013.